Journal of Solid State Chemistry 183 (2010) 1038–1045

Contents lists available at ScienceDirect

Journal of Solid State Chemistry

journal homepage: www.elsevier.com/locate/jssc

$V_{2.38}Nb_{10.7}O_{32.7}$: A V_2O_5–Nb_2O_5 mixed oxide tunnel structure related to the tetragonal tungsten bronzes

Carina Börrnert [a], Wilder Carrillo-Cabrera [a], Paul Simon [a], Hubert Langbein [b,*]

[a] Max-Planck-Institut für Chemische Physik fester Stoffe, Nöthnitzer Str. 40, D-01187 Dresden, Germany
[b] Fachrichtung Chemie und Lebensmittelchemie, Technische Universität Dresden, Helmholtz Str. 10, D-01069 Dresden, Germany

ARTICLE INFO

Article history:
Received 2 September 2009
Received in revised form
17 February 2010
Accepted 20 February 2010
Available online 10 March 2010

Keywords:
Chemical synthesis
Transmission electron microscopy
Nanostructures
Structural elucidation
Tetragonal tungsten bronze
$V_{2.38}Nb_{10.7}O_{32.7}$

ABSTRACT

A crystal structural model for the orthorhombic compound $V_{2.38}Nb_{10.7}O_{32.7}$, which is known as "$V_2Nb_9O_{27.5}$", was developed by means of selected area electron diffraction (SAED), Rietveld refinement and high resolution electron microscopy (HREM). The metastable compound is obtained by thermal decomposition of freeze-dried precursors as chain-like agglomerated nanoparticles or by reaction of V_2O_5 with fresh-precipitated Nb_2O_5 as more compact micro-scaled crystals. With the latter, it was possible to identify its structure for the first time (space group *Cmmm*). The tetragonal tungsten bronze (TTB)-type structure shows high potential for ionic intercalation, since easily reducible $[V^{5+}{}_2O^{2-}]$ units are implemented in the tunnels of a rigid niobium oxide framework.

1. Introduction

Crystalline nanoparticles are, due to their unique properties, still a common and highly stimulating research subject. Synthesis routes of crystalline nanoparticles prevalently include precursor steps [1]. This is applicable also for tetragonal tungsten bronzes (TTB) [2]. Those are known for their non-linear properties as ferroelectricity, ferroelasticity or ferromagnetism [3,4], but also for their catalytic activity and ability of ion exchange [5–7]. Therefore, the synthesis of nanoparticles with TTB structure combined with their potential for industrial application attracts considerable attention.

Apart from the thermodynamically stable VNb_9O_{25} [8] further metastable phases with the compositions "$V_2Nb_9O_{27.5}$" [9,10], $V(Nb_{11.7}V_{0.3})O_{32.5}$ [11] and $VNbO_5$ [12] are known in the quasi-binary system V_2O_5–Nb_2O_5. They can hardly be synthesized by conventional solid state reaction but via precursor decomposition at "low temperatures" varying between 500 and 700 °C for "$V_2Nb_9O_{27.5}$" and $VNbO_5$ and 900 °C for $V(Nb_{11.7}V_{0.3})O_{32.5}$. For the latter, a phase transformation into VNb_9O_{25} takes place at about 1000 °C [11]. "$V_2Nb_9O_{27.5}$" and $VNbO_5$ decompose at temperatures above 750 °C into V_2O_5 and VNb_9O_{25}. $V(Nb_{11.7}V_{0.3})O_{32.5}$ was indexed in the monoclinic crystal system with the lattice constants $a=22.22$ Å, $b=3.893$ Å, $c=17.87$ Å and $\beta=123.3$ Å [11] and its structure has been refined according to the atomic parameters of $WNb_{12}O_{33}$ [13] in the space group *C*2 [14]. The structure of $VNbO_5$ could be determined with the isostructural model of $TaVO_5$ [12]. The structure of "$V_2Nb_9O_{27.5}$" is still unknown except for its orthorhombic classification with the lattice parameters $a=17.31$ Å, $b=17.61$ Å and $c=7.939$ Å [10], which have been refined with $a=17.351$ Å, $b=17.695$ Å and $c=3.973$ Å [14,15].

All of the established structures in the quasi-binary system V_2O_5–Nb_2O_5 consist of corner sharing metal-oxygen polyhedrons. While VNb_9O_{25} and $V(Nb_{11.7}V_{0.3})O_{32.5}$ show the typical block structures of 3×3 and 3×4 $[NbO_6]$-octahedra, which are corner shared with $[VO_4]$-tetrahedra at each corner of those blocks [8,14], the structure of $VNbO_5$ consists of a loose network of both building units with large cavities [12]. A matchable structural motive of loosely connected $[MO_6]$-octahedra is also known for TTB compounds, where the cavities preferentially are occupied by alkaline or alkaline earth metals for charge balance [2,4]. But there are also modified structures of the TTB-type where the charge balance is implemented by distinct ions like it is the case in $La_{4.67}Ta_{22}O_{62}$ [16] or $Cu_{1.1}Ta_{11}O_{26.2}F_{4.8}$ [17]. Those occupations lead to a filling of the pentagonal columns within the TTB structure and thus the resulting pentagonal bipyramids are edge-shared with the octahedra. Next to it one-fifth of the former octahedra around the pentagonal cavities keeps unoccupied by the framework metal atoms and new sixfold channels are formed (Fig. 1).

We herein report on two different soft chemistry routes (SCR) for "$V_2Nb_9O_{27.5}$" resulting in nano- or microparticles. Both routes

* Corresponding author. Fax: +49 351 463 37287.
E-mail address: Hubert.Langbein@chemie.tu-dresden.de (H. Langbein).

0022-4596/$ - see front matter © 2010 Elsevier Inc. All rights reserved.
doi:10.1016/j.jssc.2010.02.018

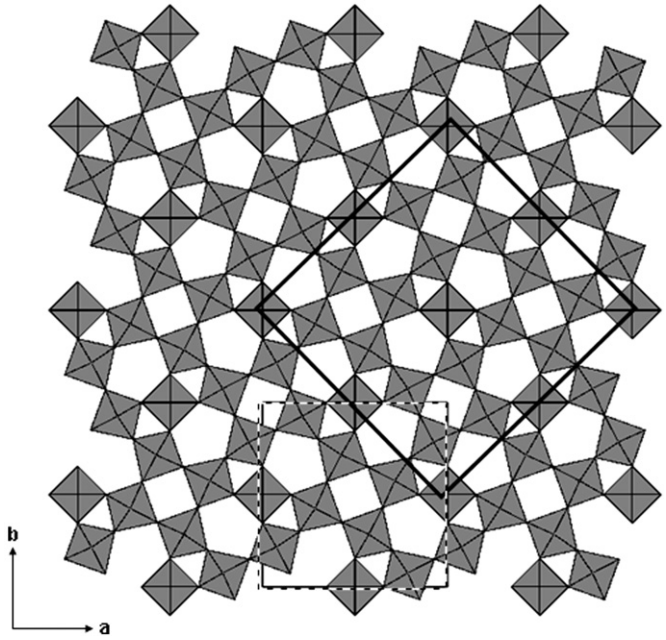

Fig. 1. Unit cells of tetragonal tungsten bronzes (dashed) and unit cell range of $Cu_{1.1}Ta_{11}O_{26.2}F_{4.8}$ presented in the TTB-structure (straight).

were already used in a similar way for the synthesis of VNb_9O_{25} [18]. The crystal structure of "$V_2Nb_9O_{27.5}$" and its particle morphology depending on the synthesis route were studied in detail by X-ray powder diffraction (XRD) and TEM. As we will show, "$V_2Nb_9O_{27.5}$" belongs to the TTB-type compounds similar to $La_{4.67}Ta_{22}O_{62}$ and $Cu_{1.1}Ta_{11}O_{26.2}F_{4.8}$. Therefore, its composition is written as $V_{2.38}Nb_{10.7}O_{32.7}$ (see below).

2. Experimental

2.1. Sample preparation

In the SCR1 the synthesis of $V_{2.38}Nb_{10.7}O_{32.7}$ was done via freeze drying: aqueous solutions of oxo-oxalato-vanadate(IV) (V_2O_5 in oxalic acid, molar ratio $V^{5+}:C_2O_4^{2-}=1:2.5$) and oxo-oxalato-niobate(V) (amorphous Nb_2O_5 in oxalic acid, molar ratio $Nb^{5+}:C_2O_4^{2-}=1:3$) of composition V:Nb=2:9 (pH=1.5) were frozen with liquid nitrogen. The frozen mixture was dried in a vacuum chamber of an Alpha 2-4 freeze-drying apparatus (Christ) at a pressure of 0.020–0.040 mbar from −33 to 17 °C. The resulting water-soluble powder was pre-decomposed by heating it at a rate of 5 K/min up to 350 °C (30 min). The phase formation followed within a second heating process (10 K/min, 5 h) to 650 °C.

The SCR2 was carried out by a reaction of V_2O_5 with fresh precipitated Nb_2O_5. A mixture of both (V:Nb=2:9) was ground (30 min). The powder was heated (10 K/min, 24 h) to 650 °C. By comparison, a solid state reaction was also carried out under terms of SCR2 with the high temperature modification of niobium oxide (H-Nb_2O_5).

2.2. Sample characterization

Monitoring the crystallization process, high-temperature XRD data were collected within a $20^\circ \le 2\theta \le 80^\circ$ range (D8 advance, Bruker), HTC, MRI, 10 K/min to 900 °C, step size 100 K, dwell 1 h (SCR1). For structural refinement, X-ray data of a well crystalline sample (SCR2) were collected within a $9^\circ \le 2\theta \le 100^\circ$ range (D5000, Siemens, Cu$K\alpha_1$).

Chemical analyses (SCR1, SCR2) were performed with a Vista inductively coupled plasma-optical emission spectrometer (Varian) for V and Nb and a Leco CHNS-932 analyzer for H. The magnetization was measured in a standard SQUID magnetometer (Quantum Design, MPMS) in various fields between 1 and 70 kOe and 1.8 and 400 K.

IR absorption spectra were taken with an FTIR-spectrograph (BioRad Excalibur FTS 3000) and Raman spectra with an Xtra NIR-laser (Toptica, 785 nm, 140 mW, CCD).

A Tecnai 10 electron microscope (FEI) was used for SAED. HREM studies were performed on a CM200 microscope (FEG/ST-Lorentz, FEI) with a line resolution of 2.0 Å and a point resolution of 2.4 Å and analyzed with the program *DigitalMicrograph* (Gatan, USA).

The particle size distribution was measured by dynamic light scattering (DLS) with the LS230 analyzer (Beckmann Coulter). The measurement was carried out with a sample dispersed in a 0.1% $Na_4P_2O_7$ solution. The BET measurement was done by using N_2 gas in a Beckmann Coulter apparatus (SCR1).

3. Results and discussion

3.1. Phase formation of mixed oxides, chemical analyses and magnetic measurements

The crystallization process of $V_{2.38}Nb_{10.7}O_{32.7}$ (SCR1) is initiated at about 600 °C and continues till 700 °C. At the temperature of 800 °C the metastable $V_{2.38}Nb_{10.7}O_{32.7}$ decomposes into thermodynamically stable VNb_9O_{25} and V_2O_5 (Fig. 2). Because of the short dwell time of 1 h at each temperature, the phase formation is incomplete and some phase mixing occurs. More crystalline single phase samples are obtained by a heating process described in the experimental part with a dwell time of 5 h at 650 °C. While the formation of $V_{2.38}Nb_{10.7}O_{32.7}$ cannot be observed for the solid state reaction of V_2O_5 with H-Nb_2O_5 [15,19], a single phase of $V_{2.38}Nb_{10.7}O_{32.7}$ is also obtained from the SCR2.

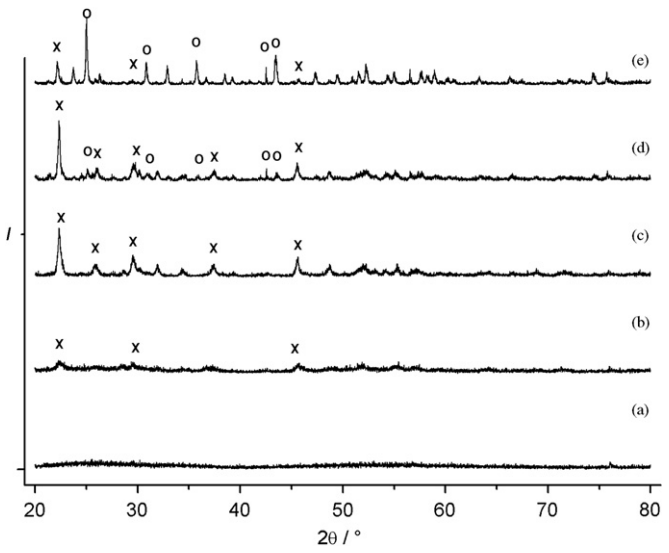

Fig. 2. High-temperature X-ray powder diffraction pattern of $V_{2.38}Nb_{10.7}O_{32.7}$ synthesized via SCR1 (heating rate 10 K/min, step size 100 K from (a) 500 °C to (e) 900 °C, 1 h holding time after each step). X marks the main peaks of the $V_{2.38}Nb_{10.7}O_{32.7}$ phase and O marks the VNb_9O_{25} phase.

XRD of SCR1 and SCR2 samples leads to similar diffraction patterns. While the broadened reflexes of the SCR1 pattern hint the particles to have a nanoscaled particle size distribution [18], the SCR2 pattern shows relatively sharp peaks and agrees well with literature data [15,19]. Because of the lower crystallinity of the SCR1 samples, their investigation was restricted to the particle characterization. The elucidation of crystal structure as a main topic of investigation was done with the SCR2 sample.

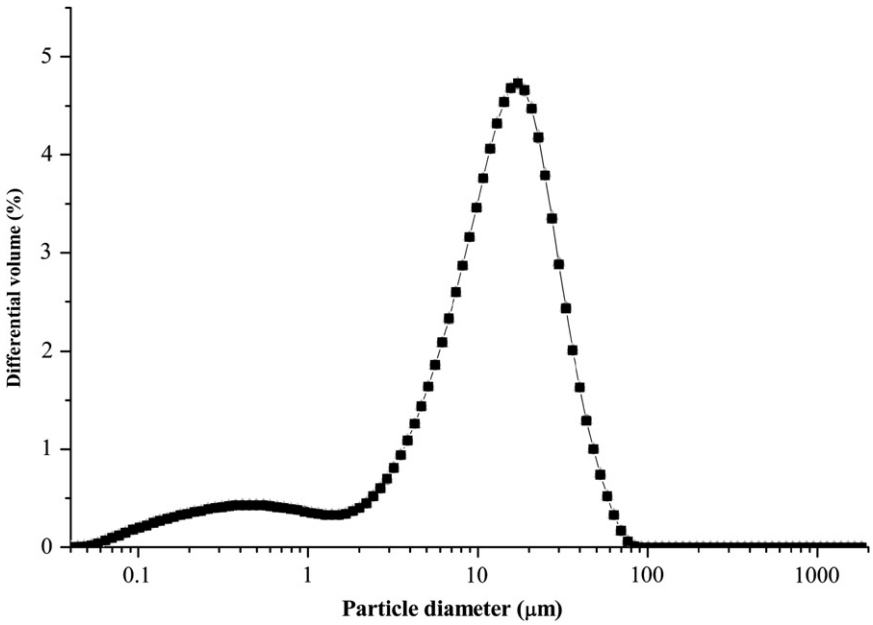

Fig. 3. Particle size distribution of $V_{2.38}Nb_{10.7}O_{32.7}$ synthesized via SCR1. Two fractions are recognizable: within the range from 2 to 100 μm and second from 10 nm to 1 μm.

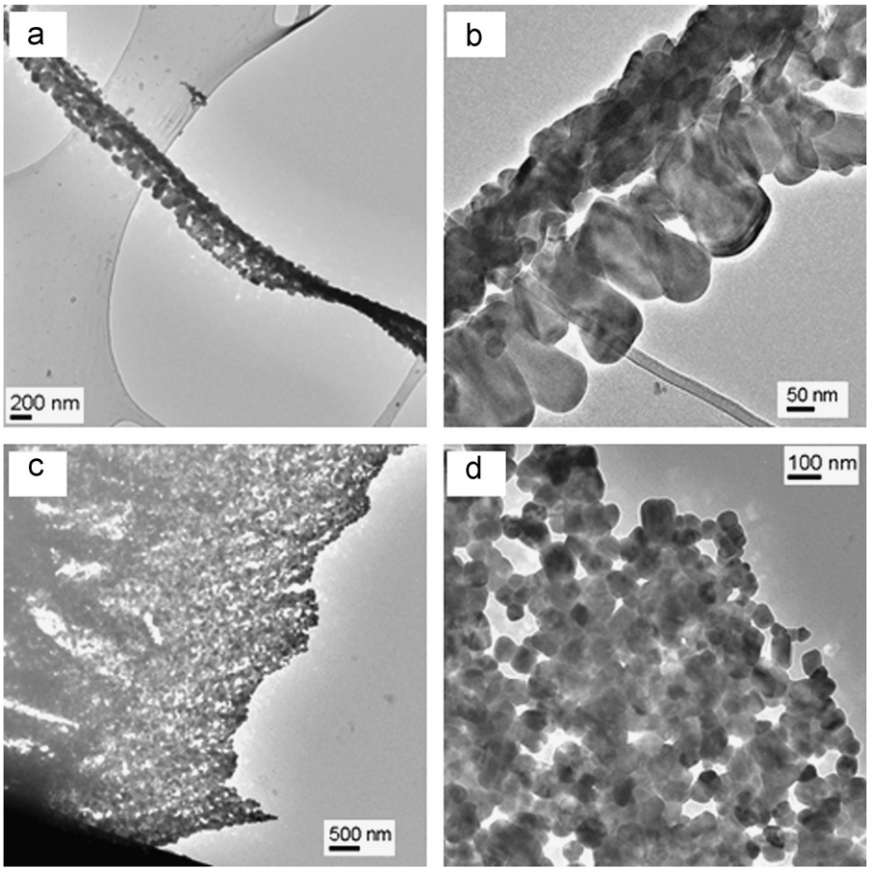

Fig. 4. (a) Isolated nanochain with several μm length and 400 nm width displaying flexible behavior indicated by bending area in the right bottom. (b) Enlarged view of 2(a) revealing spine-like morphology of nanochain. (c) Overview TEM image of microsized sheets of $V_{2.38}Nb_{10.7}O_{32.7}$ consisting of nanochains. These chains are laterally packed and linked together to form a coat of mail. (d) Zoomed micrograph of 2(c) showing interconnected nanoparticles with a size between 20 and 100 nm.

The V:Nb ratio was verified by chemical analysis to 2:9. The absence of any V(IV) species was confirmed: paramagnetic impurities of 0.39 μB/mol and an intrinsic susceptibility of $\chi_0 = 130 \times 10^{-6} \pm 20 \times 10^{-6}$ emu/mol imply less than 2.5% of all V species to be V(IV), which can be interpreted as surface or lattice defects.

3.2. Particle characterization of the SCR1 sample

The combination of low synthesis temperatures and gas formation processes during the precursor decomposition (SCR1) leads to nanoscaled particles. The particle sizes range from 2 to 100 μm and, in a second distribution fraction, from 10 nm to 1 μm

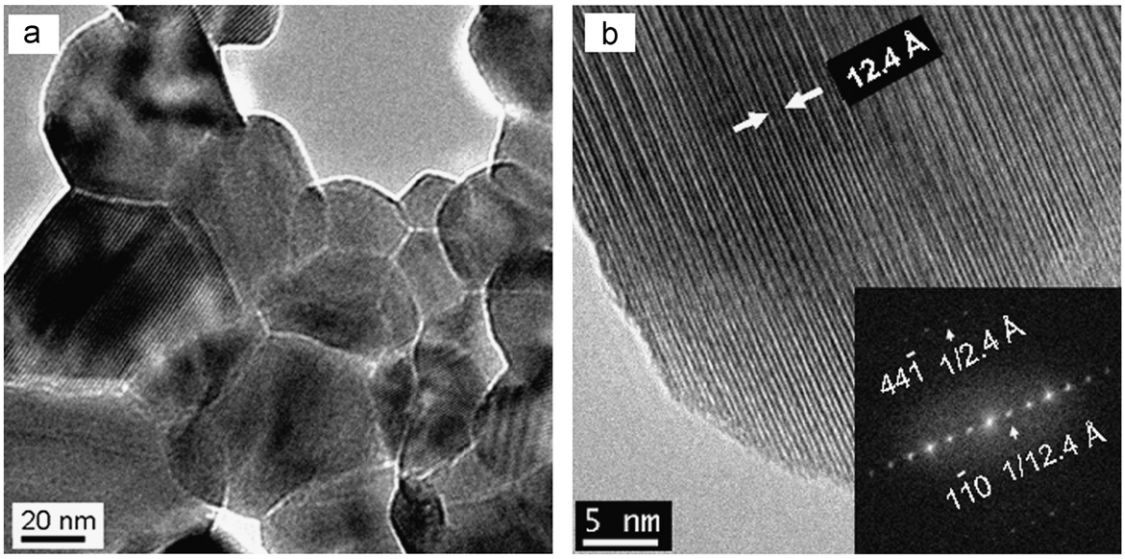

Fig. 5. (a) Middle-resolution image showing agglomeration of single crystalline nanograins within the micro-/nanoporous network. (b) HREM image of [1 1 8] zone of $V_{2.38}Nb_{10.7}O_{32.7}$ nanoparticle with corresponding FFT (inset). The diagonal strong lines indicate the (1-10) direction with a lattice spacing of 12.4 Å.

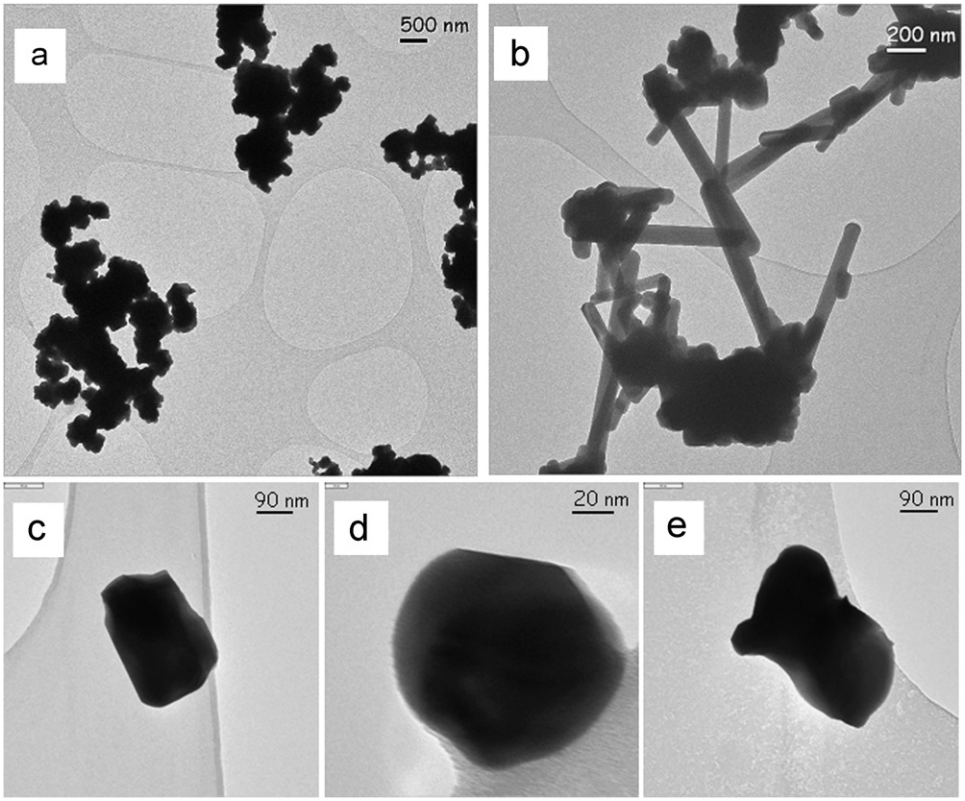

Fig. 6. TEM images from $V_{2.38}Nb_{10.7}O_{32.7}$ material prepared by SCR2. (a) TEM image showing typical aggregates of $V_{2.38}Nb_{10.7}O_{32.7}$. Crystallites appear mostly as rounded species and almost equiaxial. However, mixtures of aggregates and large single crystals (elongated along *c*-axis) were observed in a few cases, as shown in figure (b). (c)–(e) TEM images of isolated crystalline particles from which the electron diffraction patterns in Fig. 7 were taken.

(Fig. 3). A deeper understanding of this distribution was obtained from TEM and HREM experiments, which show that large particles in fact are agglomerated nanocrystallites.

The TEM images display hierarchical nanostructuring where micron-sized sheets of nanometer thickness are composed of interconnected nanochains giving rise to "mail-shirt" morphology.

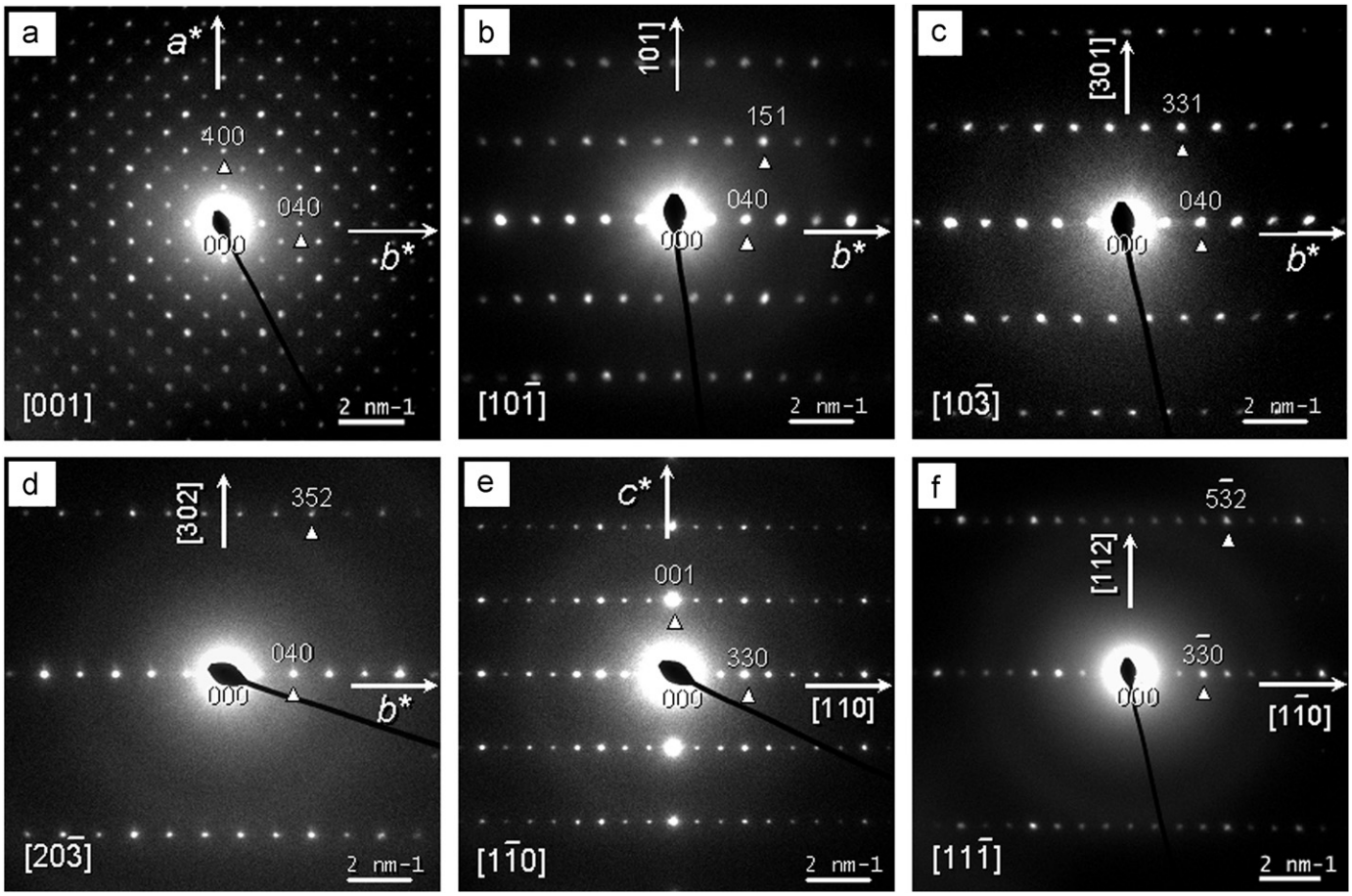

Fig. 7. SAED patterns of $V_{2.38}Nb_{10.7}O_{32.7}$ along (a) [0 0 1], (b) [1 0 −1], (c) [1 0 −3], (d) [2 0 −3], (e) [1 −1 0] and (f) [1 1 −1].

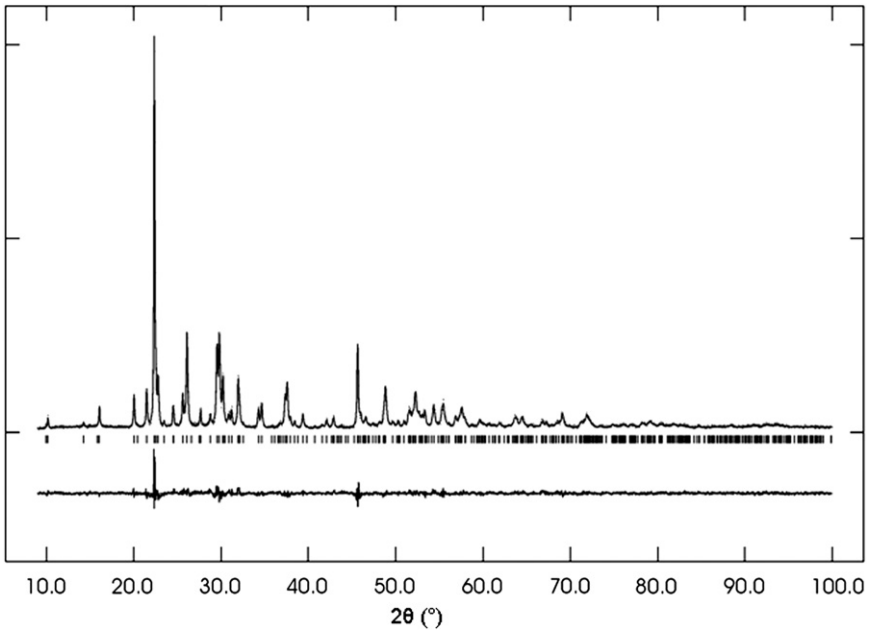

Fig. 8. Rietveld plot of the structural refinement of $V_{2.38}Nb_{10.7}O_{32.7}$ (X-ray powder pattern of a sample prepared with SCR2).

At the mesoscale, the material shows a micro-/nanoporous behavior where a statistical network is formed by interconnected nanoparticles (Fig. 4c). The size of the nanoparticles is determined to be between 20 and 200 nm (Fig. 4d). In some cases the nanograins form regular micrometer long nanowires with flexible (bended) morphology (Fig. 4a). At higher resolution, the spine-like shape of the wires is revealed where a 100 nm thick stripe is laterally decorated by rectangular shaped nanoplatelets (Fig. 4b). A closer look into the framework visualizes the agglomeration of nanograins (Fig. 5a). The nanoparticles within the network are single crystalline as revealed by HREM (Fig. 5b). In the figure the [1 1 8] zone with corresponding lattice spacings of (1-10) 12.4 Å and (44-1) 2.44 Å is represented. The minor quality and poor resolution of the electron microscopy micrograph are caused by the relatively high thickness of grains.

The specific surface area of the powder (SCR1, BET) is 7 m^2/g and agrees well with the described particle morphology.

3.3. Space group determination and crystal structure refinement of the SCR2 sample

As the particles obtained from the SCR1 were too small, single crystal SAED patterns were difficult to obtain and X-ray structure refinement was not reliable. However, the SCR2 had micro-scaled crystals of better quality (Fig. 6), and both X-ray powder data and SAED were improved. From SAED it was found that the unit cell is C-centred (Laue class *mmm*) and possible space groups are *Cmmm*, *Cmm*2, or *C*222 (Fig. 7).

As the X-ray pattern and the lattice constants of $V_{2.38}Nb_{10.7}O_{32.7}$ show good agreement with the data of the TTB-type structure $La_{4.67}Ta_{22}O_{62}$ (*Cmmm*), the Rietveld refinement was done on the basis of this structure data [20]. The results are given in Fig. 8 and Table 1. Several atoms were refined with common U_{iso} values. To avoid strong correlations between the scale factors and the U_{iso} of Nb(1)–Nb(3), the occupancies were first refined with fixed U_{iso} values (0.023). Later, the U_{iso} values were refined (with fixed occupancies). The comparison between $La^{3+}_{4.67}Ta_{22}O_{62}$ and the refined results leads to the crystallographic formula of $V^{5+}_{2.8+y}(Nb_{22-x}\square_x)O_{62+2.5(y-x)}$ with $x=0.61$ and $y=1.96$ ($\square$ = vacancy), or of $V_{2.38}Nb_{10.7}O_{32.7}$, respectively [21].

From difference Fourier maps four extra electron density peaks were found in the channels of the modified TTB structure of $La_{4.67}Ta_{22}O_{62}$. They were assigned to V(1), one 34% occupied position O(12) bonded to a 34% occupied position V(2) and a 17% occupied position V(3).

3.4. Structure description and discussion

The orthorhombic unit cell of $V_{2.38}Nb_{10.7}O_{32.7}$ is characterised by the lattice parameters $a=17.3549(5)$ Å, $b=17.6977(5)$ Å and

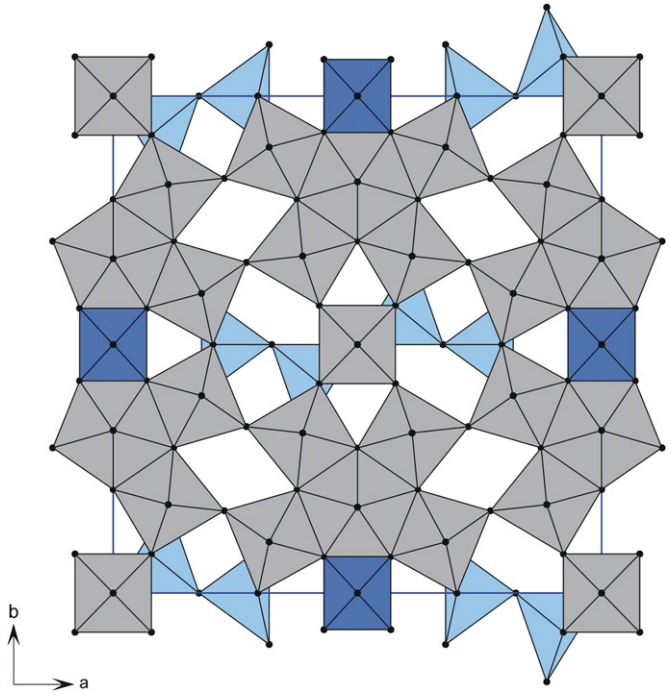

Fig. 9. [0 0 1] Projection of the $V_{2.38}Nb_{10.7}O_{32.7}$ unit cell: [NbO_6] and [NbO_7] (gray), [$V(1)O_6$] (dark blue), and [$V(2,3)O_5$] (light blue). The 1/3 occupied [$V(2,3)O_5$] polyhedra are arranged in pairs and the shown occupation of the V(3) site (each one of two local possibilities) is chosen arbitrary. (For interpretation of the references to color in this figure legend, the reader is referred to the web version of this article.)

Table 1
Atomic sites, coordinates, isotropic thermal parameters and occupancy factors for $V_{2.38}Nb_{10.7}O_{32.7}$. Several atoms were refined with common U_{iso} values. To avoid strong correlations between the scale factors and the U_{iso} of Nb(1)-Nb(3), the occupancies were first refined with fixed U_{iso} values (0.023). Afterwards, the U_{iso} values were refined (with fixed occupancies).

	WYKOFF	*x*	*y*	*z*	Occ.	U_{iso}
Nb(1)	2 *a*	0	0	0	0.90504	0.0281(17)
Nb(2)	4 *i*	0	0.67085(23)	0	0.93483	0.0248(12)
Nb(3)	8 *p*	0.18456(16)	0.39023(13)	0	0.97994	0.0257(7)
Nb(4)	16 *r*	0.11383(13)	0.81845(16)	0.0692(8)	1/2	0.0164(10)
V(1)	4 *l*	1/2	0	0.1100(27)	1/2	0.0122(32)
V(2)	4 *h*	0.2621(8)	0	1/2	0.345(6)	0.0122(32)
V(3)	8 *p*	0.1039(12)	0.0705(12)	1/2	0.1725(29)	0.0122(32)
O(1)	8 *q*	0.3176(8)	0.1019(7)	1/2	1	0.0158(10)
O(2)	8 *q*	0.6117(7)	0.6771(8)	1/2	1	0.0158(10)
O(3)	8 *p*	0.1230(7)	0.2914(8)	0	1	0.0158(10)
O(4)	8 *p*	0.0680(6)	0.5727(8)	0	1	0.0158(10)
O(5)	8 *p*	0.2734(7)	0.3339(7)	0	1	0.0158(10)
O(6)	8 *p*	0.0792(6)	0.9212(8)	0	1	0.0158(10)
O(7)	4 *j*	0	0.3235(10)	1/2	1	0.0158(10)
O(8)	4 *i*	0	0.2052(11)	0	1	0.0158(10)
O(9)	4 *g*	0.7039(10)	0	0	1	0.0158(10)
O(10)	2 *d*	0	0	1/2	1	0.0158(10)
O(11)	2 *j*	1/2	0	1/2	1	0.0158(10)
O(12)	4 *h*	0.1695(33)	0	1/2	0.345(6)	0.0158(10)

$c=3.97052(10)$ Å. The c-parameter with about 4 Å reflects a typical lattice constant for structures with corner sharing [NbO_6] octahedral [22].

The structure of $V_{2.38}Nb_{10.7}O_{32.7}$ is a modified type of a tetragonal tungsten bronze. The a–b-plane of its unit cell is 45° rotated within the a–b-plane of the TTB unit cell and the lattice constants a and b are approximately stretched with the factor $\sqrt{2}$ (Fig. 1). The structure is similar to the structure of $Cu_{1.1}Ta_{11}O_{26.2}F_{4.8}$. Fig. 9 shows the nearly square a–b-plane of the $V_{2.38}Nb_{10.7}O_{32.7}$ unit cell. It contains four [NbO_7] pentagonal bipyramids, which are edge-shared with one [VO_6] (V(1) split site) and four distorted [NbO_6] octahedra (Nb(3) and Nb(4) split site). Non-distorted [NbO_6] octahedra are located median and at the corners of the unit cell. Additionally, V(2) and V(3) are centered at edge-shared and distorted trigonal bipyramids [VO_5].

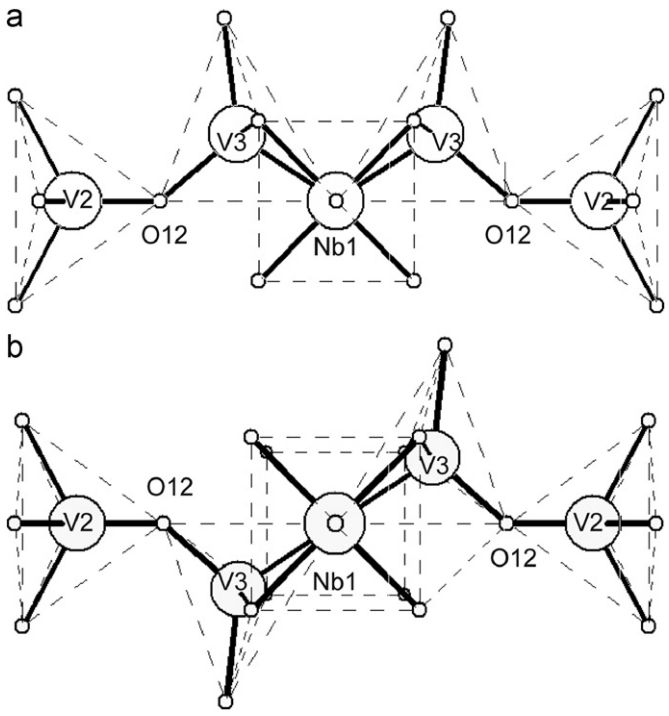

Fig. 10. Local ordered models of the partially occupied positions O(12) (occ. 34%), V(2) (4h, occ. 34%) and V(3) (8p, occ. 17%): (a) "non-inversion" symmetric model and (b) "inversion" symmetric model.

Due to the partially occupied positions O(12), V(2) and V(3), either a "non-inversion" symmetric model or an "inversion" symmetric model are possible to describe the occupation of the pentagonal tunnels of the TTB structure (Fig. 10). A local reduced symmetry caused by the split sites and by the partially occupied interstitial vanadium sites may occur and an arising symmetry reduction from *Cmmm* to *Cmm*2 possibly results. Two single IR-vibrations (1024 cm^{-1}, 972 cm^{-1}) are observed, which are also present in the Raman spectra (1016 cm^{-1}, 966 cm^{-1}) (Fig. 11). Although the values differ, this is in accordance with the absence of "inversion" symmetry [23]. A similar symmetry reduction due to a Cu split site is mentioned for the structure of $Cu_{1.1}Ta_{11}O_{26.2}F_{4.8}$ [17].

As shown earlier, the thermal treatment of different amorphous V_2O_5/Nb_2O_5 precursors with a V:Nb ratio of $\leq$1:9 at about 600 °C results in solid solutions with the structure of TT-Nb_2O_5, the low ("tief") temperature modification of Nb_2O_5. On annealing solid state mixtures of V_2O_5 and TT-Nb_2O_5 with a V:Nb ratio $\geq$2:9 at about 600 °C, independent of the composition, the compound $V_{2.38}Nb_{10.7}O_{32.7}$, crystallizes first [15]. Because of the broad diffraction peaks (see Fig. 2) and the superimposition of the most intensive peaks of $V_{2.38}Nb_{10.7}O_{32.7}$ and TT-Nb_2O_5 at about $2\theta=22.5°$, an intermediate formation of less crystalline TT-Nb_2O_5 during the annealing of amorphous $V_{2.38}Nb_{10.7}O_{32.7}$ precursors cannot be excluded.

TT-Nb_2O_5 is a disordered form of T-Nb_2O_5 with nearly the same basic atom positions [24]. The orthorhombic unit cell of T-Nb_2O_5 contains [NbO_6] octahedra and [NbO_7] pentagonal bipyramids, which are joined by sharing edges and corners in the a–b area and sharing only corners in the c-direction [25]. The structure of $V_{2.38}Nb_{10.7}O_{32.7}$, described for the first time in this paper, also contains NbO_6 octahedra and NbO_7 pentagonal

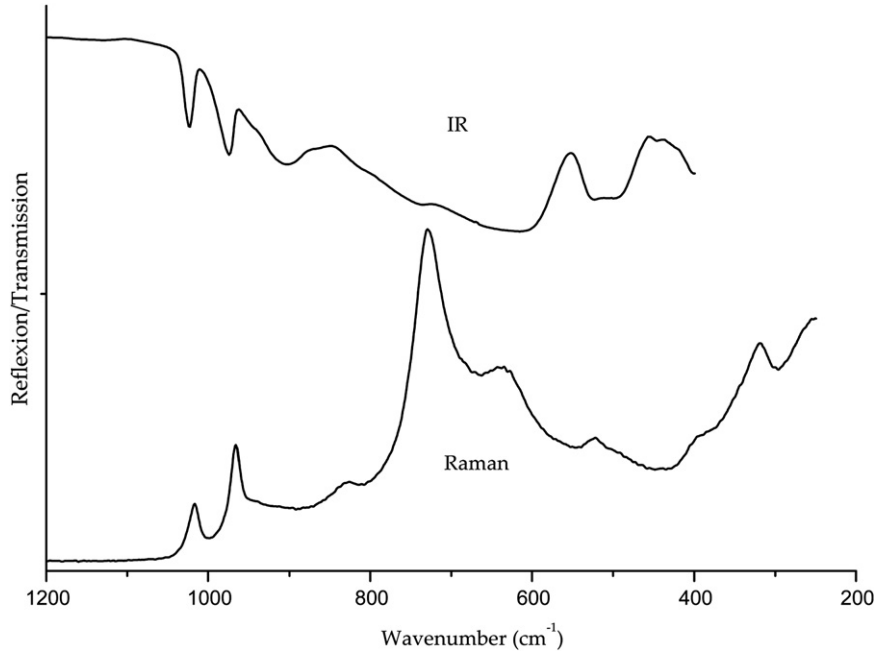

Fig. 11. IR absorption and Raman spectra of $V_{2.38}Nb_{10.7}O_{32.7}$ synthesized at 650 °C (SCR2).

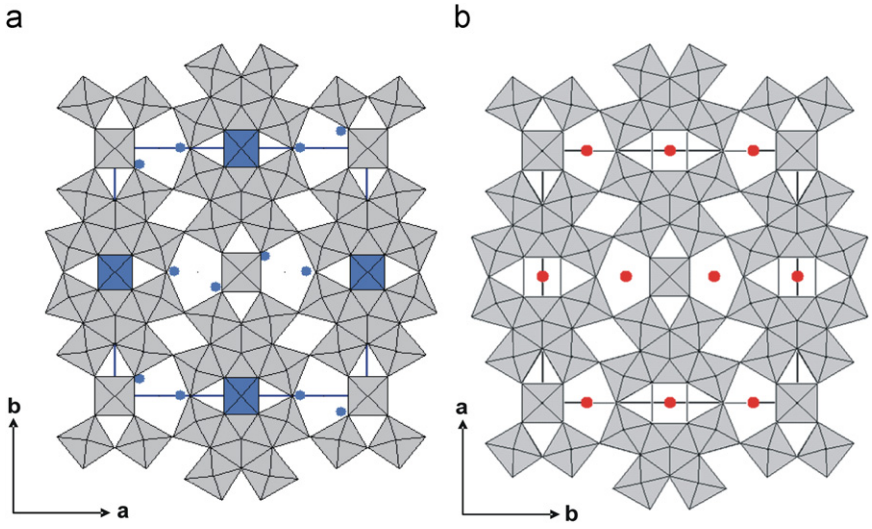

Fig. 12. Comparison of the frameworks of (a) $V_{2.38}Nb_{10.7}O_{32.7}$ with (b) $Cu_{1.1}Ta_{11}O_{26.2}F_{4.8}$ showing V (blue) and Cu (red) as "interstitial" atoms in the 4- and 5-sided tunnels. Instead of Cu^{2+}, $1/3[V^{5+}{}_2O^{2-}]$ is inserted in the 4- and 5-sided channels of $V_{2.38}Nb_{10.7}O_{32.7}$. (For interpretation of the references to color in this figure legend, the reader is referred to the web version of this article.)

bipyramids, which are joined by sharing edges and corners in the *a*–*b* area. The lattice parameter *c* nearly agrees with the *c* parameter of T-Nb_2O_5. The obvious structural relation between the starting or intermediate niobium oxide and the product $V_{2.38}Nb_{10.7}O_{32.7}$ implies that TT-Nb_2O_5 acts as a template for the crystallization of $V_{2.38}Nb_{10.7}O_{32.7}$ in a kinetically controlled reaction.

4. Conclusions

The metastable phase $V_{2.38}Nb_{10.7}O_{32.7}$ can be synthesized by a kinetically controlled reaction from an amorphous precursor or a reactive mixture of V_2O_5 and fresh precipitated amorphous Nb_2O_5. The crystal morphology strongly depends on the kind of starting powders. Well crystalline H-Nb_2O_5 is not a suitable component of the starting mixture.

$V_{2.38}Nb_{10.7}O_{32.7}$ is the first and only example of a compound with a TTB-type structure in the system V_2O_5–Nb_2O_5. Usually, TTB structures consist of a loose network of metal oxide octahedra [MO_6] with large cavities, which are occupied either by alkaline or alkaline earth metals or, in a modified TTB structure, by distinct ions as La^{3+} in $La_{4.67}Ta_{22}O_{62}$, Cu^{2+} in $Cu_{1.1}Ta_{11}O_{26.2}F_{4.8}$ or 1/3 $[V_2^{5+}O^{2-}]$ in $V_{2.38}Nb_{10.7}O_{32.7}$ (Fig. 12). The presence of the easily reducible V(V) in the tunnels of the network results in interesting properties as the facility for intercalation of alkaline ions. Present studies show that it is possible to intercalate Li^+ ions from a LiI/CH_3CN solution in the structure of $V_{2.38}Nb_{10.7}O_{32.7}$ [14]. This may hint $V_{2.38}Nb_{10.7}O_{32.7}$ to be an interesting compound for electrochemical applications or applications as catalyst.

Acknowledgments

The authors are grateful to Dr. W. Fichter, Dr. K. Ahlborn and Prof. Dr. Guth for performing the HT-XRD and BET analysis. We also thank Dr. C. Krafft for the Raman investigations as well as Prof. Dr. Lichte for supporting the TEM studies. We gratefully acknowledge Dr. G. Auffermann for elemental analyses and Dr. W. Schnelle for measurements of the magnetism. Finally, we like to thank Dr. U. Schwarz for helpful discussions.

References

[1] H.-P. Baldus, M. Jansen, Angew. Chem. 109 (1997) 329–343.
[2] A. Magneli, Arkiv Foer Kemi 1 (1949) 213–221.
[3] A. Simon, J. Ravez, C.R. Chim. 9 (2006) 1268–1276.
[4] B.P. Jamieson, S.C. Abrahams, J.L. Bernstein, J. Chem. Phys. 50 (1969) 4352–4362.
[5] A. Bialas, B. Borzecka-Prokop, A. Weselucha-Birczynska, J. Camra, M. Najbar, Catal. Today 119 (2007) 194–198.
[6] P. Botella, E. Garcia-Gonzalez, J.M. Lopez Nieto, J.M. Gonzalez-Calbet, J. Solid State Sci. 7 (2005) 507–519.
[7] A. Kuhn, H. Bashir, A.L. Dos Santos, J.L. Acosta, F. Garcia-Alvarado, J. Solid State Chem. 177 (2004) 2366–2372.
[8] M. Casais, E. Gutierrez-Puebla, M.A. Monge, I. Rasines, C. Ruiz-Valero, J. Solid State Chem. 102 (1993) 261–266.
[9] O. Yamaguchi, Y. Mukaida, H. Shigeta, Z. Anorg. Allg. Chem. 574 (1989) 235–238.
[10] O. Yamaguchi, Y. Mukaida, H. Shigeta, Adv. Powder Technol. 1 (1990) 3–12.
[11] T. Mayer-Uhma, H. Langbein, Thermochem. Acta 447 (2006) 178–183.
[12] J.M. Amarilla, B. Casal, E. Ruiz-Hitzky, J. Mater. Chem. 6 (6) (1996) 1005–1011.
[13] R.S. Roth, A.D. Wadsley, Acta Crystallogr. 19 (1965) 32–38.
[14] C. Bergner, Niobreiche Oxidphasen des quasibinären Systems V_2O_5-Nb_2O_5 - Phasenbildung und Intercalationsverhalten, Diploma thesis, Technische Universität Dresden (FRG) (2007).
[15] H. Langbein, T. Mayer-Uhma, Mater. Res. Bull. 44 (2009) 654–659.
[16] U. Schaffrath, R. Gruehn, Z. Anorg. Allg. Chem. 573 (1989) 107–118.
[17] C. Askeljung, M. Lubdberg, M. Sundberg, Int. J. Inorg. Mater. 2 (2000) 469–476.
[18] C. Bergner, V. Vashook, S. Leoni, H. Langbein, J. Solid State Chem. 182 (2009) 2053–2060.
[19] P. Tabero, E. Filipek, M. Piz, Cent. Eur. J. Chem. 7 (2009) 222–227.
[20] A.C. Larson, R.B. Von Dreele, Program *GSAS*, Los Alamos Nation al Laboratory Report LAUR, 1994, pp. 86–748.
[21] Crystallographic data: *Cmmm* (*Cmm2*), $Z=2$, cell parameters: [Å]: $a=17.3549(5)$, $b=17.6977(5)$, $c=3.97052(10)$, $V=1219.52(6)$ Å^3, $fw=1637.88$ g mol^{-1}, $\rho_{calc}=4.460$ g cm^{-3}, $\lambda=1.5418$ Å, $2\theta=9$–100°, $\Delta 2\theta=0.008^\circ$, no. of reflections: 398, $F_{000}=1508.6$, $R_b=0.0571$, $\omega R_P=0.0925$; CSD number: 420781.
[22] M. Sundberg, B.O. Marinder, J. Solid State Chem. 84 (1990) 23–38.
[23] M. Schmidt, B. Ewald, Yu. Prots, R. Cardoso-Gil, M. Armbrüster, I. Loa, L. Zhang, Ya-Xi. Huang, U. Schwarz, R. Kniep, Z. Anorg. Allg. Chem. 630 (2004) 655–662.
[24] J.G. Weissmann, E.I. Ko, P. Wynblatt, J.M. Howe, Chem. Mater. 1 (1989) 187–193.
[25] K. Kato, S. Tamura, Acta Crystallogr. B 31 (1975) 673–677.